Ion-wake field inside a glass box

Mudi Chen,[1,*] Michael Dropmann,[1,2] Bo Zhang,[1] Lorin S. Matthews,[1] and Truell W. Hyde[1,†]

[1]*Center for Astrophysics, Space Physics and Engineering Research, Baylor University, One Bear Place 97310, Waco, Texas 76798-7310, USA*

[2]*Institute of Space Systems, University of Stuttgart, Raumfahrtzentrum Baden-Württemberg, Pfaffenwaldring 29,70569 Stuttgart, Germany*

(Received 15 April 2016; revised manuscript received 18 July 2016; published 2 September 2016)

The confinement provided by a glass box is proving ideal for the formation of vertically aligned structures and a convenient method for controlling the number of dust particles comprising these dust structures as well as their sizes and shapes. In this paper, the electronic confinement of the glass box is mapped, and the particle interactions between the particle pairs inside the glass box are measured. The ion-wake field is shown to exist within the glass box, and its vertical and horizontal extents are measured.

DOI: 10.1103/PhysRevE.94.033201

I. INTRODUCTION

A dusty plasma [1] is best described as a weakly ionized gas containing electrons, ions, neutral atoms, and small solid particles, usually consisting of micron-size spheres. Due to the high thermal speed of the electrons, these microparticles are usually negatively charged [2,3]. The charge on any single particle can vary from a few hundred to several 10^6 elementary charges [4], depending on particle size and plasma conditions. In an experimental setting on the earth, the particles can be levitated against the force of gravity in the plasma sheath near the powered electrode by a self-induced electric field. Depending on the external confinement, one-dimensional (1D) to three-dimensional (3D) dust structures can be formed [5–8]. Placing a glass box on the lower electrode is a common method for providing such confinement and is used to create dust clusters with different numbers of particles from one to several dozens by tuning the radio-frequency (rf) power. Once established, transitions from 1D to two-dimensional (2D) zigzag, 2D to 3D helical structures, and helical structures to layered structures [9] are easily obtained.

Particles also interact directly with one another through screened Coulomb repulsion and indirectly by altering the ion flow, which determines the plasma screening and ion-wake field. The ion-wake effect has been studied both theoretically [10–17] and experimentally [18–21]. Research has shown that charged dust particles tend to align with the ion flow [11,14]. Upstream particles focus the ions at a point beneath them, and downstream particles are attracted by the positive space charge region created due to this ion focusing. A nonreciprocal interaction [10,20] between the upstream and the downstream particles is a signature property of the ion-wake effect. In this case, upstream particles dominate the motion of downstream particles, whereas the reverse effect is so small that it can often be considered negligible. Recent simulation studies [22] also indicate that the downstream particles can become discharged by this interaction between the upstream and the downstream particles.

As noted, a glass box confinement has proven ideal for the formation of vertically aligned 1D, 2D, and 3D structures, which are difficult to obtain under other types of confinement. However, a study of the role the ion-wake effect plays within such a confinement or whether the ion-wake field exists at all in this environment is conducted here. Given the strong confinement produced by the glass box and the direct interaction between the particles, an investigation of the ion-wake effect has long been ignored, leaving a proper explanation of the underlying physics sorely needed.

In this paper, under the confinement created by a glass box, the interaction between the particles and the ion-wake field as it pertains to vertically aligned single particle chains is examined. Section II provides a short description of the experimental setup employed, whereas Sec. III shows data collected mapping both the accelerations provided by the confining forces within the glass box as well as the mutual particle accelerations as a function of the particles' locations relative to each other. A discussion of these data, which shows the existence of the wake field, is given in Sec. IV with conclusions presented in Sec. V.

II. EXPERIMENTAL SETUP

The experiment described here was performed in a modified gaseous electronics conference (GEC) rf cell, filled with argon at a pressure of 6.67 ± 0.10 Pa. An rf electrical field was produced by a pair of capacitively coupled electrodes 8 cm in diameter, situated one above the other, and separated by a distance of 2.54 cm. The upper electrode was grounded, whereas the lower electrode was powered by a rf generator at a constant frequency of 13.56 MHz. The amplitude of the input rf signal was 2 W. An open-ended glass box of dimension $1.27 \times 1.07 \times 1.07\,\mathrm{cm}^3$ (height × width × length) with 2 mm wall thickness was placed at the center of the lower electrode. Melamine formaldehyde spheres having a manufacturer-specified mass density of $1.514\,\mathrm{g/cm}^3$ and a diameter of $12.00 \pm 0.09\,\mu$m were used. A dust dropper was employed to introduce the particles into the glass box where they were illuminated by a vertical sheet of laser light. The particles' positions were recorded at 500 or 1200 frames per second (fps) using a side-mounted high-speed CCD (Photron) camera and a microscope lens. In order to manipulate isolated particles, optical radiation from a Coherent Verdi V-5 laser was introduced into the chamber using an adjustable optical system (see Fig. 1). The power supplied to the laser was user controlled and held between 0.01 and 1.50 W. In previous experiments conducted at CASPER [23], an electron temperature of 5 eV

*mudi_chen@baylor.edu

†truell_hyde@baylor.edu

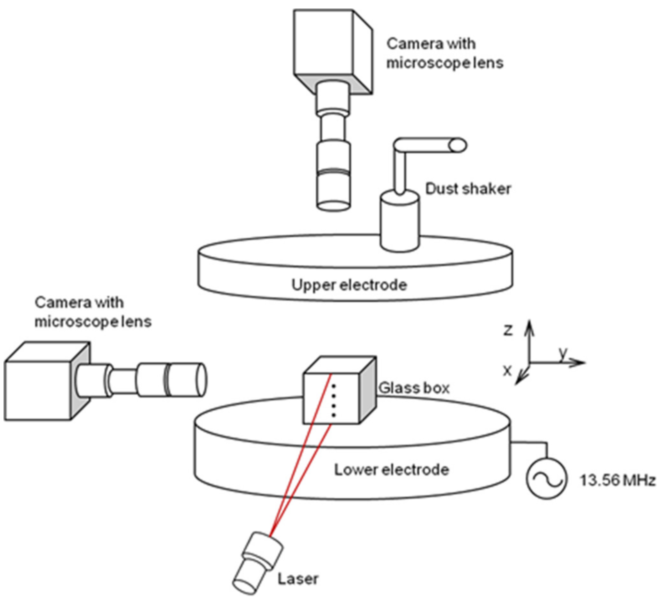

FIG. 1. Experimental setup. The top electrode is grounded whereas the bottom electrode is powered. The separation distance between the electrodes is 2.54 cm. The open-ended glass box shown has outer dimensions of $1.27 \times 1.07 \times 1.07\,\mathrm{cm}^3$. A Coherent Verdi V-5 laser is employed to perturb individual particles, the motion of which is then captured using a Photron CCD high-speed camera (side view).

and a plasma bulk density of $2 \times 10^{15}\,\mathrm{m}^{-3}$ was measured under the same operating conditions.

III. DATA COLLECTION AND RESULTS

A. Confinement

It is difficult to measure the particle-particle interaction inside a glass box due to the unknown nature of the confinement. Since dust particles are levitated in either the sheath or the presheath region within the small volume of the glass box, common diagnostic methods cannot in general be employed due to the perturbations they create. For example, introducing a probe into this environment changes both the electric field inside the box as well as the charge on the dust particles. As such, only techniques producing very small perturbations may be employed to measure the plasma environment around the dust particles. In this case, a free-falling-particle technique was applied to measure the confinement produced by the glass box. In this technique, the dust particle itself is used as a probe to measure the forces affecting the particles and create a map of the overall confinement. In our experiment, a few hundreds of dust particles were dropped from the dust dropper located above the upper electrode into the glass box with individual particle motion recorded at 1200 fps. A MATLAB-based algorithm [24] for particle detection was employed to identify the particles in each frame of the data collected, which were then linked using the Hungarian algorithm [22]. The details of this algorithm can be found in the Appendix.

The resulting particle trajectories were examined to eliminate any faulty data. Trajectories exhibiting discontinuities in their calculated accelerations were removed as were

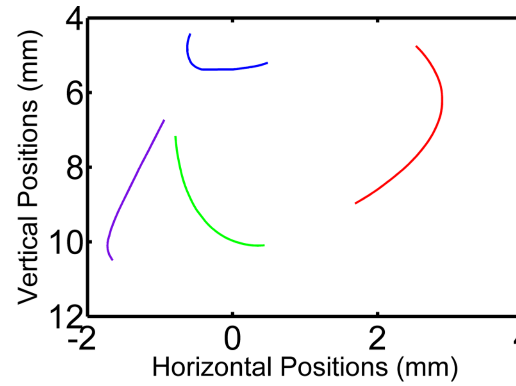

FIG. 2. Sample trajectories for four different particles (indicated by the red, green, purple, and blue lines).

trajectories exhibiting minimal particle movement since both of these are usually associated with noise falsely interpreted as particles. Particle-particle interactions were managed by establishing a minimum allowable distance between detected particles. For this case, it was 1 mm. Sample valid particle trajectories are shown in Fig. 2. These trajectories were taken from different drops. The particle trajectories were fit by a third order polynomial, and the first and second order difference quotients were used to determine the velocities and accelerations in both the vertical $(\dot{Z},\ddot{Z})$ and the horizontal $(\dot{X},\ddot{X})$ directions.

Assuming that only gas drag, confining electrostatic forces, and gravity are acting on the particles, the equations of motion are given by

$$m_d \ddot{Z} = -\beta \dot{Z} + Q_d E_z - m_d g, \tag{1}$$
$$m_d \ddot{X} = -\beta \dot{X} + Q_d E_x, \tag{2}$$

where m_d is the mass of the dust particle, β is the gas drag coefficient, g is the acceleration due to gravity ($9.81\,\mathrm{m/s^2}$), Q_d is the charge on the dust particle, and E_z and E_x are the electric fields in the vertical and horizontal directions. In this case, the drag is considered to be due to collisions with the neutral gas particles with the gas drag coefficient β defined as

$$\beta = \delta \frac{4\pi}{3} a^2 N m_n \bar{c}_n, \tag{3}$$

where a is the radius of the dust particle, N is the neutral gas number density, m_n is the mass of the neutral gas atoms (argon), and the coefficient δ accounts for the microscopic mechanism governing collisions between the gas atom and the surface of the dust particle. For this experiment, with melamine formaldehyde particles and argon gas, δ has been determined to be 1.44 as reported in Refs. [25,26]. Finally, $\bar{c}_n$ is the thermal speed and given by

$$\bar{c}_n = \sqrt{\frac{8kT}{\pi m_n}}, \tag{4}$$

where k is the Boltzmann constant and T is the temperature. For the given experiment, Eqs. (3) and (4) yield a value for $\beta = 9.26 \times 10^{-12}\,\mathrm{N\,m^{-1}\,s}$. This coefficient was also measured experimentally [27], giving $\beta = (9.77 \pm 2.56) \times$

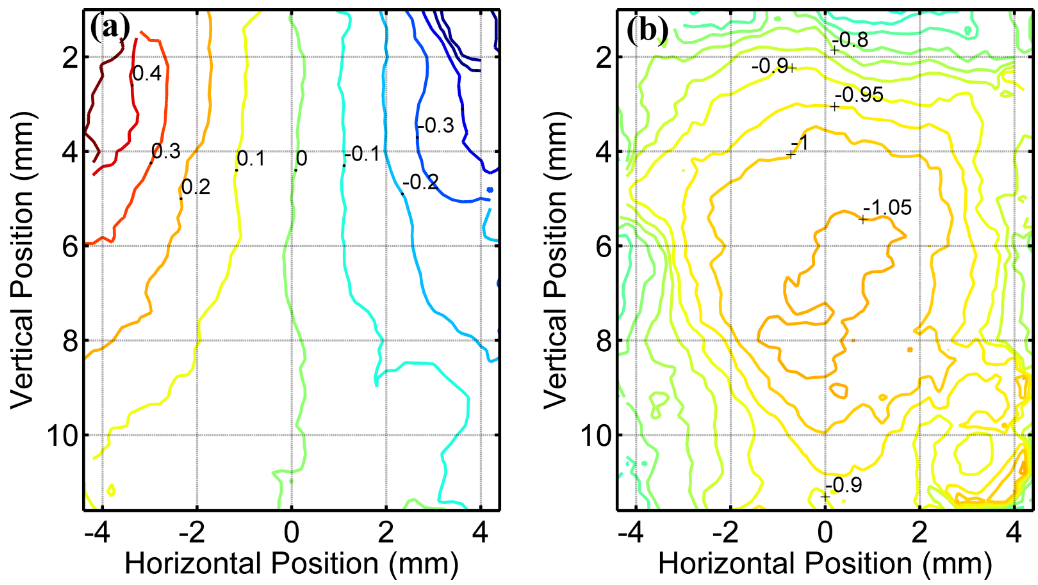

FIG. 3. Maps of the (a) horizontal and (b) vertical accelerations due to the electrostatic forces measured within the box. Experiments shown were run at 6.67 Pa argon gas pressure and 2 W rf power. Particle acceleration is given as a multiple of g, and the negative sign indicates upward acceleration. In the vertical direction, the distance is measured from the top of the glass box. In the horizontal direction, distance is measured from the center of the box.

10^{-12} N m^{-1} s, in good agreement with the analytical value. The analytical value was used in all following calculations.

In the sheath, ions in general have a large velocity directed toward the lower electrode, allowing estimation of the ion drag force using [28]

$$F_I = -\pi a^2 m_i n_i {v_i}^2. \tag{5}$$

Obtaining the ion density n_i and velocity v_i from a numerical fluid model of the plasma sheath for similar operating conditions [29,30], the force due to ion drag is found to be 0.2%–1.5% of the force due to gravity over the range of the particle heights. It indicates that the ion drag force is at least one order of magnitude smaller than the confinement force and therefore may be considered negligible here. Meanwhile, since no external thermal gradient is applied to the system, the thermophoretic forces may be also considered negligible [25] and are not included.

The components of acceleration due to the confinement $Q_d E_x/m_d$ and $Q_d E_z/m_d$ are found by subtracting the calculated acceleration due to drag from the measured acceleration (and subtracting the acceleration due to gravity in the vertical direction). These calculated particle accelerations were mapped as a function of position within the box. Since this paper focuses on 1D vertically aligned dust particle structures confined at the center of a glass box, only acceleration maps for the central region of the glass box were generated as shown in Figs. 3(a) and 3(b). This figure covers the horizontal and vertical ranges of all recorded particle trajectories with the vertical displacement measured from the top of the glass box and the horizontal displacement measured from the center of the box. The mapping used a grid spacing of 0.1 mm, and the acceleration at each grid point was calculated as the average acceleration for all data points within a radius of $R = 0.05$ mm of each grid point. To minimize effects due to particle interactions, only data points from particles at least 1 mm away from any other particle were included.

Figure 3(a) shows the horizontal acceleration of the dust particles. This acceleration is always directed toward the center of the box with the greatest acceleration of approximately $0.5g$ observed at the top edge. As shown, in the central region of the box (-1 mm $\leqslant x \leqslant$ 1 mm, -2 mm $\leqslant z \leqslant -6.5$ mm) the horizontal confinement force can be treated as a linear force with a restoring constant of $-0.11 \pm 0.01 m_d g$ mm^{-1}.

Figure 3(b) shows the vertical acceleration map for the dust particles. Particles can only levitate in the region where their vertical acceleration is greater than or equal to the acceleration due to gravity. In contrast to the conditions within the plasma sheath formed without a box, under the experimental parameters shown, the vertical confinement force inside the glass box does not increase monotonically as a particle approaches the lower powered electrode. A maximum vertical acceleration in magnitude of $\sim 1.05g$ is found at the middle of the box (-2 mm $\leqslant x \leqslant$ 2 mm) with an extended vertical region (5.5 mm $\leqslant z \leqslant$ 9 mm) where the acceleration is approximately $-1g$. As such, a 1D dust string consisting of more than two particles can only be formed in such a region. For the operating parameters used to generate the data shown in Fig. 2, the longest particle chain observed consisted of 11 particles spanning a vertical region of 9.7 mm. It should be noted that, unlike the case without a box where the radii of the particles within such a vertical structure are often different, a particle chain formed inside the box consists of nearly identically sized particles.

The vertical levitation region is highly dependent on the system's operating parameters. For example, decreasing the rf power decreases both the extent of the region as well as the magnitude of the confining force until at some critical points, particles can no longer be levitated and those closest to the lower electrode are removed. Thus, the number of particles

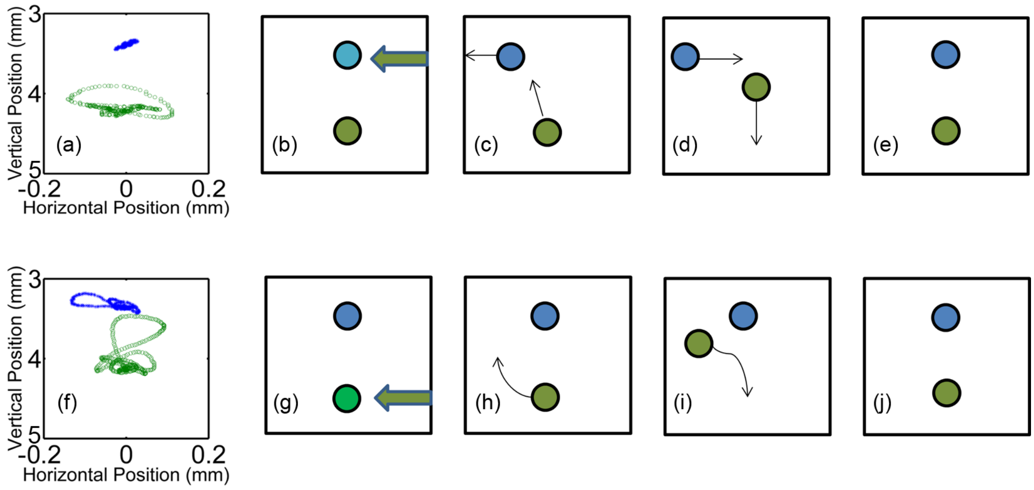

FIG. 4. Perturbed motion of particles within a particle pair. Blue represents the top particle of the pair whereas green represents the bottom particle. The (a) experimental data and (b)–(e) representative cartoon when only the top particle is disturbed; the (f) experimental data and (g)–(j) representative cartoon when only the bottom particle is disturbed. The vertical axis and horizontal axis in (a) and (f) represent the distance to the top and the middle of the box, respectively.

comprising a vertically aligned particle chain can be controlled using the rf power.

B. Particle-particle interaction within a two-particle chain

With a proper measurement of the accelerations due to the confinement of the glass box, it is possible to investigate the particle-particle interactions inside the box. To accomplish this, a Coherent VERDI G5 laser was employed to perturb individual particles in a two-particle vertical chain, and their subsequent motion was recorded using a high-speed camera running at 500 fps. In the simplest case, a particle pair was formed, and an individual particle was pushed horizontally using a pulsed laser beam of 100 ms duration with 10 mW power. The diameter of the beam spot was approximately 50 μm, and the particles were initially aligned vertically with an interparticle separation distance of 0.80 $\pm$ 0.05 mm. Due to the short heating time, low laser power, and small diameter of the beam as compared to the interparticle distance, each particle could easily be perturbed separately. Figure 4 shows the experimental data as well as a cartoon of the particle motion while separately perturbing the top or bottom particle.

As shown in Figs. 4(b)–4(e), pushing the top particle to the left [Fig. 4(b)] causes the bottom particle to move upward and slightly to the left [Fig. 4(c)]. As the horizontal displacement of the top particle increases, the confinement produced by the box eventually forces it back toward equilibrium [Fig. 4(d)], resulting in the bottom particle returning to its original position [Fig. 4(e)]. Perturbation of the bottom particle in an analogous manner is illustrated in Figs. 4(g)–4(j). Once the bottom particle is removed from its equilibrium position, it immediately moves upward as shown in Fig. 4(h). During this time, the top particle remains stationary until the interparticle distance is smaller than 550 μm at which point it is repelled slightly upward and to the right. Once the bottom particle returns to its equilibrium position (again due to the horizontal confinement), it drops quickly beneath the top particle as seen in Fig. 4(i). Finally, in Fig. 4(j), the particle pair resumes its stable configuration after a short time of exhibiting damped oscillations.

The total force acting on the particles once the laser beam is removed consists of the confinement force, the neutral drag force, and the particle-particle interaction force,

$$\boldsymbol{F}_{\text{total}} = \boldsymbol{F}_{\text{conf}} + \boldsymbol{F}_{\text{drag}} + \boldsymbol{F}_{\text{inter}}, \tag{6}$$

since for the reasons described earlier, the ion drag force and the thermophoretic force can be considered negligible. The total force is calculated by tracking the motion of particles. Therefore, the particle-particle interaction force can be calculated by using the total measured force and subtracting the confinement force (as determined above) and the neutral drag force, which is assumed to be of the form

$$\boldsymbol{F}_{\text{drag}} = -\beta \boldsymbol{v}, \tag{7}$$

Figure 5 shows the displacement [Figs. 5(a) and 5(c)] and the calculated acceleration [Figs. 5(b) and 5(d)] of both particles due to the particle-particle interaction force in the horizontal direction. Negative quantities represent movement directed toward the left, whereas positive numbers represent motion to the right. Note that the negative acceleration of the illuminated particle persists for some time after the laser is turned off. This is assumed to be due to the photophoretic force caused by particle heating [31]. As shown, when the top particle is perturbed from its equilibrium position [Fig. 5(a)], the bottom particle follows in the same direction over a short range (100 μm) before reversing direction to oscillate about its equilibrium position.

When the bottom particle is pushed to left as shown in Fig. 5(c), the top particle remains at its original position before being repelled slightly to the right. This phenomenon confirms the assumption that the initial motion observed for the bottom particle when the top particle was pushed [see the trajectory during the first 0.1 s in Fig. 5(a)] was not caused by the laser. The damped particle oscillation also allows the neutral gas

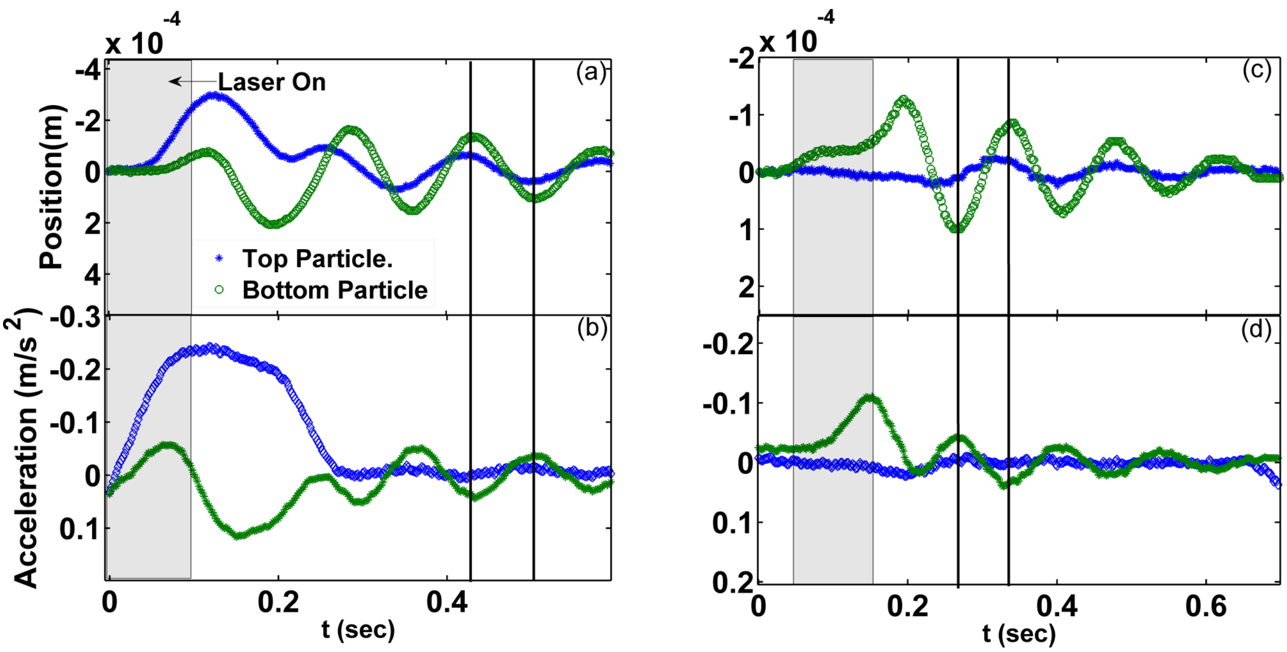

FIG. 5. Particle motion and acceleration due to the particle-particle interaction force in the horizontal direction. (a) Motion and (b) acceleration for perturbation of the top particle and (c) motion and (d) acceleration for perturbation of the bottom particle for the conditions described in the text. The shaded region indicates the time during which the laser illuminated the particle. The vertical lines indicate the positions and accelerations of the particles at corresponding times.

drag coefficient β to be calculated using [32],

$$\ddot{X} + \beta\dot{X} + \omega_0^2 X = 0, \tag{8}$$

where X is the horizontal displacement from the equilibrium position and ω_0 is the natural frequency of the horizontal potential well. The value of β determined in this manner is $(8.97 \pm 1.15) \times 10^{-12}\,\mathrm{N\,m^{-1}\,s}$, also in agreement with analytically calculated results.

Figures 5(b) and 5(d) show the acceleration created by the force imparted by the laser and resulting interparticle interactions. In the first case, the top particle was initially given an acceleration of $0.3\,\mathrm{m/s^2}$ to the left by the laser. The bottom particle followed the top particle, was displaced to the left, and experienced a maximum acceleration of $0.05\,\mathrm{m/s^2}$. As the particles returned to oscillate about their equilibrium positions after 0.3 s, it can be seen that the acceleration of the top particle was almost zero, whereas the bottom particle still had a maximum acceleration of $0.04\,\mathrm{m/s^2}$ directed toward the top particle as indicated by the vertical lines showing the correlation between the positive force for a negative displacement. Upon perturbation of the lower particle, Fig. 5(d), the top particle was repelled, moving to right for the first 0.2 s during the time that the bottom particle approached it from below and left. By the time the bottom particle returned to its equilibrium position, the interaction force acting on the top particle was almost negligible, although the bottom particle continued to exhibit an attractive interaction, again indicated by the vertical lines.

Using the perturbation method described, acceleration maps for the interparticle interaction between the top and the bottom particles were generated by separately perturbing particles with varying laser powers between 0.01and 0.50 W. The region where the data were collected was overlaid with a grid with a spacing of 0.1 mm, and the average acceleration was calculated for all data points within a radius of 0.05 mm of each grid point. Accelerations were calculated only for regions containing at least five data points. In all cases, the coordinate origin was centered on the position of the top particle, indicated by the blue dot, whereas the y axis and the x axis represent the vertical and horizontal interparticle separations, respectively. At equilibrium, the bottom particle is located at [0,0.79], indicated by the green dot, measured with respect to the location of the top particle.

In Figs. 6(a) and 6(c), positive values indicate horizontal acceleration to the right, whereas in Figs. 6(b) and 6(d), positive values represent downward vertical acceleration. Figures 6(a) and 6(b) provide interaction maps for the force of the top particle acting on the bottom particle (generated by perturbing the top particle), whereas the data shown in Figs. 6(c) and 6(d) were obtained by perturbing the bottom particle and show the force exerted on the top particle by the bottom particle at the specific separations. Taken together, these provide the interparticle interactions between the bottom and the top particles. Note that the horizontal axes are asymmetric in the two cases as the bottom particle is to the right of the top particle when the top particle is perturbed, whereas the bottom particle is to the left of the top particle when the bottom particle is perturbed. The white regions out of the contours indicate lack of data.

In Fig. 6(a), the horizontal acceleration of the bottom particle is shown obtained for the region where the interparticle distance was larger than 0.4 mm. The horizontal accelerations are always directed toward the midline directly beneath the top particle, indicating that the bottom particle experiences a horizontal attractive interparticle interaction across this region. The strongest attractive acceleration $-0.05\,\mathrm{m/s^2}$ is observed

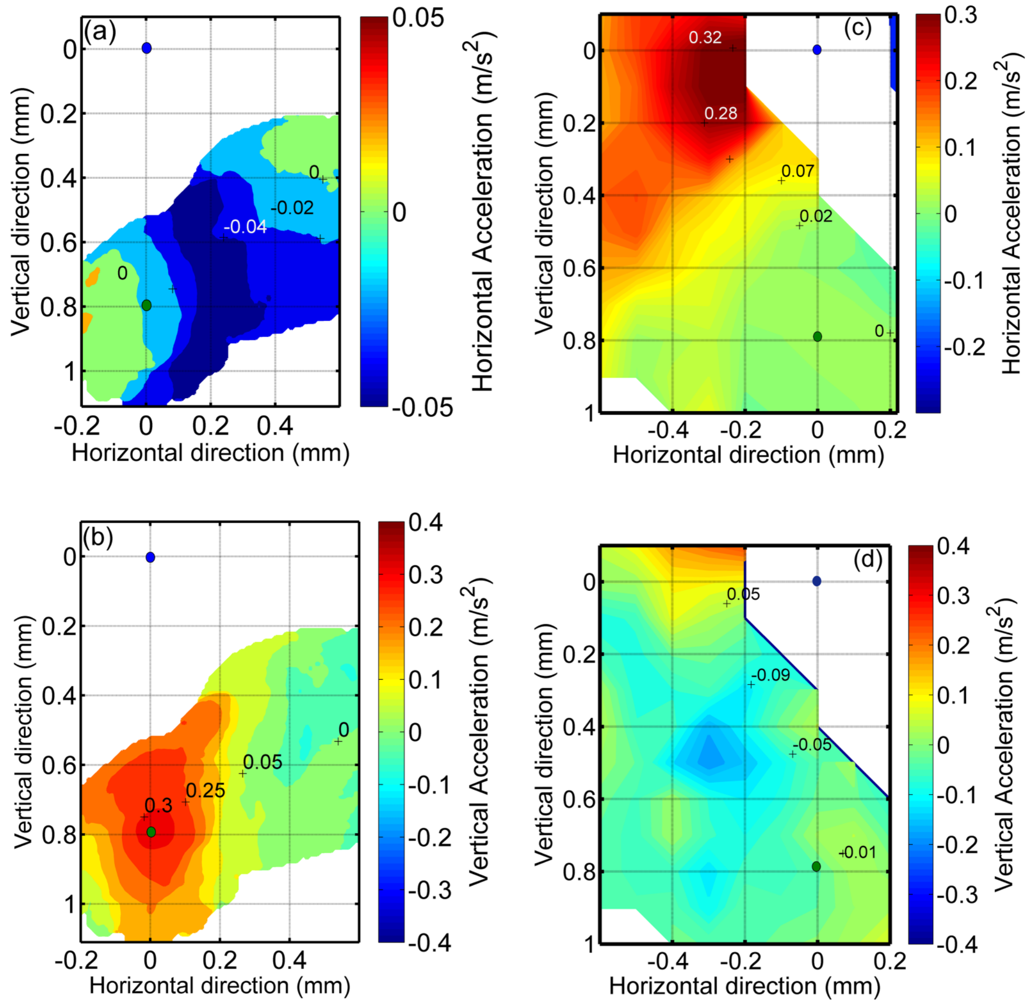

FIG. 6. Maps of the acceleration due to interparticle interaction. (a) and (b) show the horizontal and vertical accelerations of the bottom particle due to the interaction from the top particle when the top particle is perturbed. (c) and (d) show the horizontal and vertical accelerations of the top particle due to the interaction from the bottom particle when the bottom particle is perturbed. In all cases, [0,0] is the position of the top particle, and the x and y axes give the horizontal and vertical displacements of the bottom particle from the top particle. Positive acceleration values indicate rightward and downward accelerations, respectively. The blue point indicates the position of the top particle at the point [0,0], whereas the green circle indicates the equilibrium position of the bottom particle [0,0.079].

approximately 0.3 mm away from the midline beneath the top particle, which is in agreement with measurements made by Hebner *et al.* [19] and Hebner and Riley [33] using two particles with different masses approaching each other under a cutout confinement. As seen in Fig. 6(b), the vertical acceleration of the bottom particle is always downward, showing there is only a repulsive interaction from the top to the bottom particle. The maximum downward acceleration $0.31\ \mathrm{m/s^2}$ is observed at approximately [0,0.79], which coincides with the particle's equilibrium position. As shown in Fig. 6(c), the horizontal acceleration provided from the bottom to the top particle is almost zero when the bottom particle is at its equilibrium positions. All the accelerations in Fig. 6(c) are positive (to the right) whereas the bottom particle is at the left side of the top particle. This indicates that the bottom particle repels the top particle to the right. Note that the top particle can only be repelled by the bottom one and that repulsive acceleration increases with decreasing interparticle distance. In Fig. 6(d), the bottom particle causes the top particle to have an upward (negative) acceleration when their vertical separation is larger than 0.2 mm. In this region, the repulsive interaction from bottom to top is increasing with decreasing distance with a maximum magnitude of less than $0.1\ \mathrm{m/s^2}$. It is interesting to note that the top particle gains a downward acceleration when the bottom particle is close to it and on the same horizontal plane.

IV. DISCUSSION

As shown in Figs. 5(a) and 5(c), in the horizontal direction, the top particle of a vertically aligned two-particle chain attracts the bottom particle, whereas the bottom particle exerts little to no force on the top particle at the same relative positions. Only repulsive horizontal force can be observed on the top particle from the bottom particle in Fig. 6(c). At the same time, Figs. 5(b) and 5(d) show that, although both the top and the bottom particles in the chain repel each other in the vertical direction, the acceleration of the top particle is

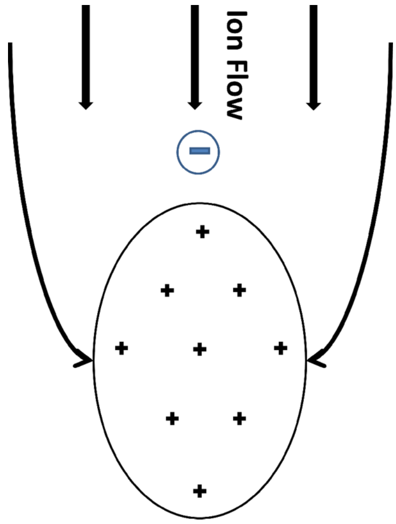

FIG. 7. Scheme of the ion wake. The blue circle is the dust particle.

much smaller than the acceleration of the bottom particle. The top particle exerts a maximum downward vertical acceleration (and therefore force) of $0.31\ \mathrm{m/s^2}$ on the bottom particle when it is at a point 0.79 mm directly below the top particle. This point coincides with the equilibrium position of the lower particle. The corresponding acceleration of the top particle in the equilibrium configuration is less than $0.01\ \mathrm{m/s^2}$. In other words, the interaction between the top and the bottom particle is nonreciprocal in both the horizontal and the vertical directions.

This nonreciprocal attractive interaction in the horizontal direction has been previously observed in particle-pair experiments under similar operating conditions but without a glass box confinement [19,20]. It is generally explained using the ion-wake effect where a positive ion-focusing region is formed beneath the upper particle due to the ion flow as shown in Fig. 7. The positive space charge region, the location of which is determined by the upstream particle, can attract the downstream particle, whereas the downstream particle can only repel the upstream particle since both are negatively charged. The positive space charge region also causes the downstream particle to charge less negatively as there is an enhanced ion impact on the downstream particle. This discharging effect has been measured experimentally [21] as well as predicted numerically [22,34] but again without a glass box confinement. Given that a nonreciprocal interaction is considered to be a primary indicator of the ion-wake field effect, the experiments here prove the existence of an ion-wake field within the box.

It is interesting to note that due to the strong confinement provided by the box, an attractive interaction can only be observed close to the midline beneath the top particle, which in these experiments spans a horizontal region of $-0.3\ \mathrm{mm} \leqslant x \leqslant 0.3\ \mathrm{mm}$. Outside this region, the horizontal confinement produced by the glass box is much larger than the observed attractive effect, which may explain why the existence of the ion-wake effect within a glass box has remained in question for such a long time. In the vertical direction, the wake field effect is much more apparent. As shown in Figs. 6(b) and 6(d), the bottom particle always experiences a downward interaction while providing only a small interaction acceleration on the top particle, particularly at vertical distances longer than 0.7 mm. This implies that the nonreciprocal interparticle ratio (i.e., the interaction between the upstream and the downstream divided by the interaction between the downstream and the upstream particles) may be quite large (approximately 5–60). This is interesting since for experiments without a glass box, this ratio is much smaller (approximately five to ten) [21]. The largest value found for this ratio in there is $R = 60$, observed when particles are near their equilibrium positions (top particle at [0,0] and bottom particle at [0,0.79]). The downward acceleration gained by the top particle when the bottom particle is close to the top particle may be due to the resolution of our mapping technique.

The largest source of uncertainty for this particular series of experiments is due to the variation in particle size and mass. The manufacturer provides a standard deviation value for each particle size, but our measurements show a larger range than is reported. For example, for the batch of 8.89 μm particles used in this experiment (with a manufacturer stated standard deviation of 0.09 μm) the measured size range as determined by scanning electron microscopy is [7.1–9.8] μm.

In the first experiment, the horizontal confinement measured at a specific point of $0.1g$ ($0.981\ \mathrm{m/s^2}$) results in an uncertainty of $\pm 0.02\ \mathrm{m/s^2}$, whereas in the vertical direction, a measured value of $1.05g$ ($10.305\ \mathrm{m/s^2}$) has an uncertainty of $\pm 0.01\ \mathrm{m/s^2}$. The error caused by the mass variation is on the order of $10^{-2}\ \mathrm{m/s^2}$. Due to the small velocity (10^{-4} m/s) involved, the error in the calculation of the neutral drag is on the order of $10^{-3}\ \mathrm{m/s^2}$, on the same order as the error caused by the uncertainty in the position measurements due to the size of the image pixel size (7 μm). Therefore, the main source of error should be due to the mass variation. In order to minimize this error these experiments were designed to average over a large number of trajectories (40 drops for each parameter).

V. CONCLUSIONS

A particle free-fall technique has been employed to map the confinement produced by a glass box placed on the lower powered electrode of a GEC rf reference cell. Interaction maps between the top and the bottom particles and the bottom and the top particles of a two-particle chain were generated employing a laser beam to perturb each individual particle. A nonreciprocal particle interaction was observed in both the horizontal and the vertical directions, confirming the existence of an ion-wake field within the glass box. It was shown that, for this case, the predicted attractive horizontal nonreciprocal phenomenon can only be observed near the midline of the box due to the existence of the strong inherent confinement forces produced by the box, whereas in the vertical direction, the nonreciprocal ratio is much greater than that observed without a glass box confinement. This explains why the existence of an ion-wake field in a glass box has long been in question; the horizontal attractive interaction between a particle and the ion-wake field is much smaller than that provided by the confinement force for most regions within the box. However, at the midline of the box, these become comparable, and in the vertical direction, the effect of the ion-wake field can become large enough to play an integral role in determining the position of the downstream particle. A representative example of this is the extended levitation region observed where dust particles experience an upward electrical force approximately equal to that of the gravitational force. This "flat" confinement region is the key factor for forming long 1D vertically aligned dust particle structures.

The above shows that additional confinement data will be required in order to enhance the overall resolution and provide a more detailed interaction map. Once completed, this will allow investigation of the interaction between the ion-wake and the particle structure formation. This research is currently underway and will be reported in a future publication.

ACKNOWLEDGMENT

Support from NSF Grant No. 1262031 and NSF/ DOE Grant No. 1414523 is gratefully acknowledged.

APPENDIX

The image analysis method used here is based on the MATLAB program “SIMPLE TRACKER” by Tinevez.

Particle tracking consists of rebuilding the trajectories of one or more particles as they move in time. This requires the particles to be identified and tracked from frame to frame. The Hungarian algorithm has long been used to solve this assignment problem. It was developed and published in 1955 by Kuhn [35], who gave it the name “Hungarian method” because the algorithm was largely based on the earlier works of two Hungarian mathematicians: Kőnig and Egerváry [35].

In this method, links are created among particle pairs having the shortest Euclidean distance. A maximal value for particle links is also specified by the user: Two particles will not be linked (even if they are the remaining closest pair) if their distance is larger than this value. The Hungarian algorithm ensures that the sum of the pair distances is minimized over all particles between two frames. The following steps outline how to apply the Hungarian method.

Step 0. Create an $n \times m$ matrix (the cost matrix) in which each element represents the distance from one of the n particles in one frame to one of the m particles of the next frame. Transpose the matrix, if necessary, so that there are at least as many columns as rows, and let $k = \min(n,m)$.

Step 1. For each row of the matrix, find the smallest element, and subtract it from every other element in its row.

Step 2. Find a zero (Z) in the resulting matrix. If there is no previously starred zero in the row or column, star Z. Repeat for each element in the matrix.

Step 3. Cover each column containing a starred zero. If k columns are covered, the starred zeros describe a complete set of unique assignments. In this case, go to DONE, otherwise, proceed to Step 4.

Step 4. Find a noncovered zero, and prime it. If there is no starred zero in the row containing this primed zero, go to Step 5. Otherwise, cover this row, and uncover the column containing the starred zero. Continue in this manner until there are no uncovered zeros left. Save the smallest uncovered value, and go to Step 6.

Step 5. Construct a series of alternating primed and starred zeros as follows. Let Z_0 represent the uncovered primed zero found in Step 4. Let Z_1 denote the starred zero in the column of Z_0 (if any). Let Z_2 denote the primed zero in the row of Z_1 (there will always be one). Continue until the series terminates at a primed zero that has no starred zero in its column. Unstar each starred zero of the series, star each primed zero of the series, erase all primes, and uncover every line in the matrix. Return to Step 3.

Step 6. Add the value found in Step 4 to every element of each covered row, and subtract it from every element of each uncovered column. Return to Step 4 without altering any stars, primes, or covered lines.

DONE. Assignment pairs are indicated by the positions of the starred zeros in the cost matrix. If $C(i,j)$ is a starred zero, then the element associated with row i is assigned to the element associated with column j.

[1] G. E. Morfill and A. V. Ivlev, Rev. Mod. Phys. **81**, 1353 (2009).
[2] V. A. Schweigert, I. V. Schweigert, A. Melzer, A. Homann, and A. Piel, Phys. Rev. E **54**, 4155 (1996).
[3] J. Chu and L. I, Phys. Rev. Lett. **72**, 4009 (1994).
[4] W. Ruben, V. Sushkov, H. Kersten, V. Ikkurthi, R. Schneider, and R. Hippler, New J. Phys. **12**, 033036 (2010).
[5] V. M. Bedanov and F. M. Peeters, Phys. Rev. B **49**, 2667 (1994).
[6] L. Candido, J. Rino, N. Studart, and F. M. Peeters, J. Phys.: Condens. Matter **10**, 11627 (1998).
[7] A. Melzer, Phys. Rev. E **73**, 056404 (2006).
[8] T. E. Sheridan, Phys. Plasmas **19**, 057302 (2012).
[9] T. W. Hyde, J. Kong, and L. S. Matthews, Phys. Rev. E **87**, 053106 (2013).
[10] G. Lapenta, Phys. Plasmas **6**, 1442 (1999).
[11] G. Lapenta, Phys. Rev. E **66**, 026409 (2002).
[12] W. J. Miloch, S. V. Vladimirov, H. L. Pecseli, and J. Trulsen, Phys. Rev. E **77**, 065401 (2008).
[13] W. J. Miloch, J. Trulsen, and H. L. Pecseli, Phys. Rev. E **77**, 056408 (2008).
[14] W. J. Miloch, Plasma Phys. Controlled Fusion **52**, 124004 (2010).
[15] C. T. N. Willis, J. E. Allen, M. Coppins, and M. Bacharis, Phys. Rev. E **84**, 046410 (2011).
[16] I. H. Hutchinson, Phys. Rev. E **85**, 066409 (2012).
[17] I. H. Hutchinson, Phys. Rev. Lett. **107**, 095001 (2011).
[18] U. Konopka, G. E. Morfill, and L. Ratke, Phys. Rev. Lett. **84**, 891 (2000).
[19] G. A. Hebner, M. E. Riley, and B. M. Marder, Phys. Rev. E **68**, 016403 (2003).
[20] A. Melzer, V. A. Schweigert, and A. Piel, Phys. Rev. Lett. **83**, 3194 (1999).

[21] J. Carstensen, F. Greiner, D. Block, J. Schablinski, W. J. Miloch, and A. Piel, Phys. Plasmas **19**, 033702 (2012).

[22] W. J. Miloch and D. Block, Phys. Plasmas, **19**, 123703 (2012).

[23] J. R. Creel, Master's thesis, Baylor University, 2010.

[24] J. Y. Tinevez, SIMPLE TRACKER, http://www.mathworks.com/matlabcentral/fileexchange/34040-simple-tracker.

[25] V. Land, L. S. Matthews, T. W. Hyde, and D. Bolser, Phys. Rev. E **81**, 056402 (2010).

[26] B. Liu, J. Goree, V. Nosenko, and L. Boufendi, Phys. Plasmas **10**, 9 (2003).

[27] M. Dropmann, R. Laufer, G. Herdrich, L. S. Matthews, and T. W. Hyde, Phys. Rev. E **92**, 023107 (2015).

[28] V. E. Fortov, A. G. Khrapak, S. A. Khrapak, V. I. Molotkov, and O. F. Petrov, Phys.-Usp. **47**, 447 (2004).

[29] J. Carstensen, F. Haase, H. Jung, B. Tadsen, S. Groth, F. Greiner, and A. Piel, IEEE Trans. Plasma Sci. **41**, 764 (2013).

[30] A. Douglass, V. Land, L. Matthews, and T. Hyde, Phys. Plasmas **18**, 083706 (2011).

[31] G. Wurm, J. Teiser, A. Bischoff, H. Haack, and J. Roszjar, Icarus **208**, 482 (2010).

[32] Z. Zhang, K. Qiao, J. Kong, L. Matthews, and T. Hyde, Phys. Rev. E **82**, 036401 (2010).

[33] G. A. Hebner and M. E. Riley, Phys. Rev. E **69**, 026405 (2004).

[34] P. Ludwig, W. J. Miloch, H. Kaherlt, and M. Bonitz, New J. Phys. **14**, 053016 (2012).

[35] H. W. Kuhn, Nav. Res. Logist. Q. **2**, 83 (1955).